



# Mesoscopic quantum mechanics: mesoscopic solid-state qubits and quantum measurements

D.V. Averin  
Stony Brook University, SUNY

## Outline

### 1. Mesoscopic condensed-matter qubits

#### ``Single-particle'' physics and qubits

- Coulomb-blockade phenomena
- Cooper-pair and atomic qubits
- Electron (quantum dot) and FQHE quasiparticle (anti-dot) qubits

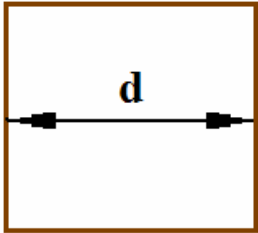
#### Generic superconductor (flux, charge-flux, ``phase'') qubits

### 2. Decoherence in mesoscopic qubits

### 3. Quantum measurements and mesoscopic detectors

### 4. Topological quantum computation

## Coulomb-blockade phenomena



Mesoscopic conductor:

$$d \sim 0.1 - 1.0 \mu\text{m} \gg a, \lambda_{\text{TF}}$$

$$H = E_C (n - q)^2 + \sum_j \varepsilon_j n_j, \quad E_C \equiv e^2 / 2C,$$

$$n_j = c_j^+ c_j, \quad n = \sum_j n_j.$$

Estimates:

$$C \approx 4\pi\varepsilon\varepsilon_0 d \approx 10^{-16} \text{F}, \quad E_C \approx 1.0 \text{meV} (10\text{K});$$

$$\delta \equiv \varepsilon_{j+1} - \varepsilon_j \approx E_F / N, \quad \delta \ll E_C.$$

PROCEEDINGS  
OF THE  
AMERICAN PHYSICAL SOCIETY.

MINUTES OF THE FORTY-SEVENTH MEETING.

A REGULAR meeting of the Physical Society was held in the Palmer Laboratory of Princeton University on Saturday, October 23, 1909. President Henry Crew presided.

The following papers were presented :

1. The Relationship Between Entropy and Time. W. S. FRANKLIN.
2. The Lorentz Shortening: an Apparent Paradox. GILBERT N. LEWIS.
3. Ionization Produced by Entladungsstrahlen and Experiments on the Nature of the Radiation. ELIZABETH R. LAIRD.
4. The Effect of  $\text{NO}_3$  and Al on the Uranyl Bands and of Ca and Temperature on Neodymium Bands. W. W. STRONG.
5. The Octave Overtone from Tuning Forks. D. C. MILLER.
6. The Electrostatic Effect of a Changing Magnetic Field. J. M. KUEHNE.
7. A Modification of the Thomson-Wilson Method of Determining the Elementary Electrical Charge, and the Most Probable Value of that Charge. R. A. MILLIKAN.
8. Polarization of Röntgen Rays. WM. R. HAM.
9. A New Radiant Emission from the Spark. R. W. WOOD.
10. The Dependence of the Photo-electric Current on the Wavelength of Incident Light. F. K. RICHTMYER.
11. Kinetic Energy of Thermions. O. W. RICHARDSON.
12. Contact Difference of Potential in the Magnetic Field. E. P. ADAMS.
13. A Neglected Form of Relativity. D. F. COMSTOCK.
14. The Relation between the Velocity of Light and the Velocity of its Source. R. C. TOLMAN.
15. The Radiation from Platinum. (By title.) A. TROWBRIDGE.
16. A Characteristic of Spectral Energy Curves. (By title.) W. W. COBLENTZ.
17. The Depth of Complete Scattering of Kathode Rays in Lead and the Variation of the Depth with Velocity of the Rays. WM. R. HAM.

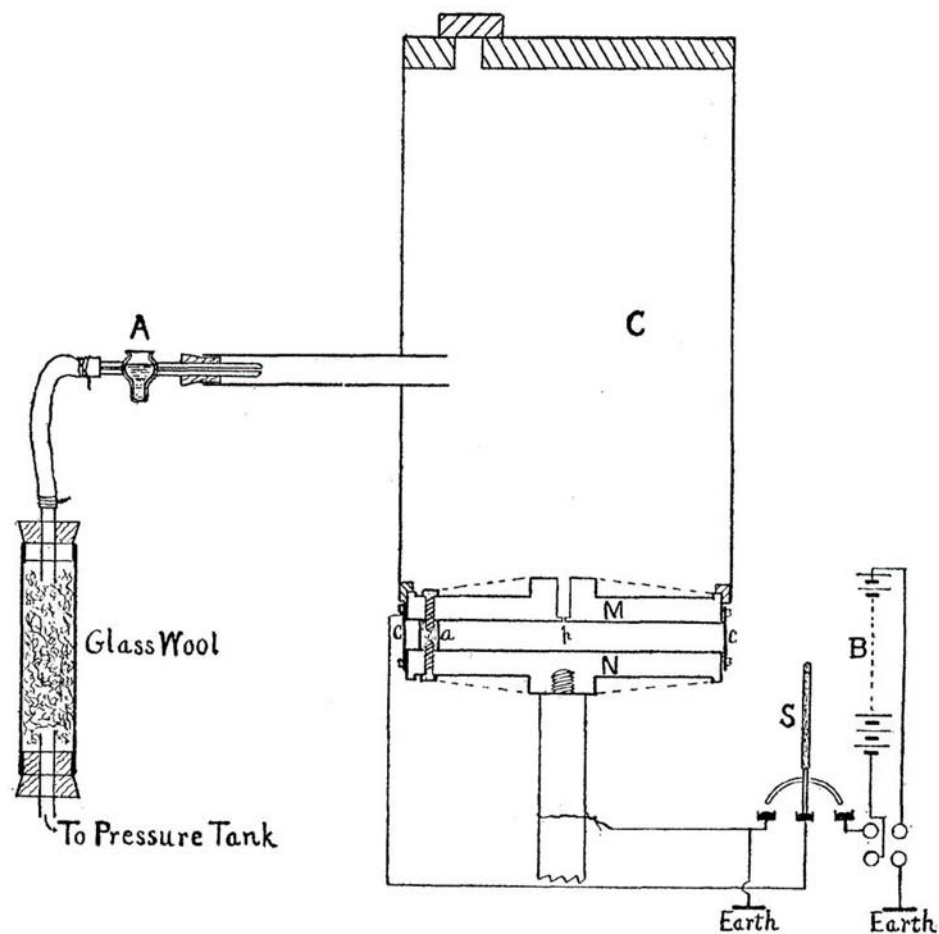
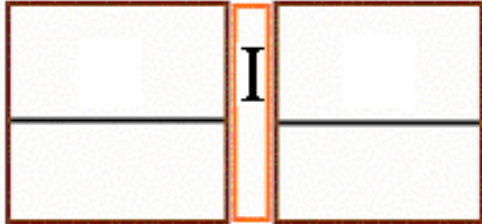


Fig. 1.

R.A. Millikan, *Phys. Rev. (Ser. I)*  
32, 349 (1911).

## Tunneling



$$H_T = \sum_{jk} (T_{jk} c_j^+ c_k + T_{jk}^* c_k^+ c_j).$$

**|j> to continuum:**

$$\Gamma_j = (2\pi / \hbar) \sum_k |T_{jk}|^2 \delta(\varepsilon_j - \varepsilon_k + \Delta U) (1 - f(\varepsilon_k))$$

$$= (2\pi / \hbar) |T|^2 \rho_k (1 - f(\varepsilon_j + \Delta U)).$$

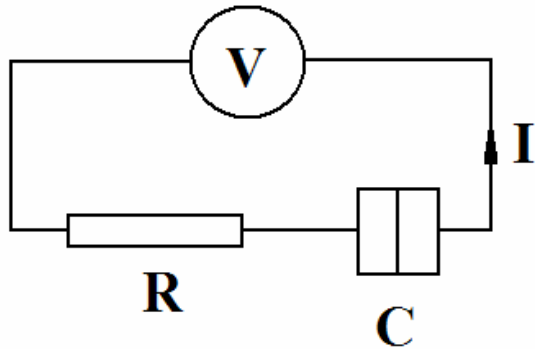
**continuum to continuum:**

$$\Gamma(\Delta U) = \sum_j \Gamma_j f(\varepsilon_j) = (G / e^2) [\Delta U / (1 - \exp(-\Delta U / T))]$$

$$G = 1 / R_T = (4\pi e^2 / \hbar) |T|^2 \rho_k \rho_j.$$

**Example:**  $\Delta U = eV$ :  $I = e[\Gamma(\Delta U) - \Gamma(-\Delta U)] = V / R_T.$

## Single junction



### Coulomb blockade

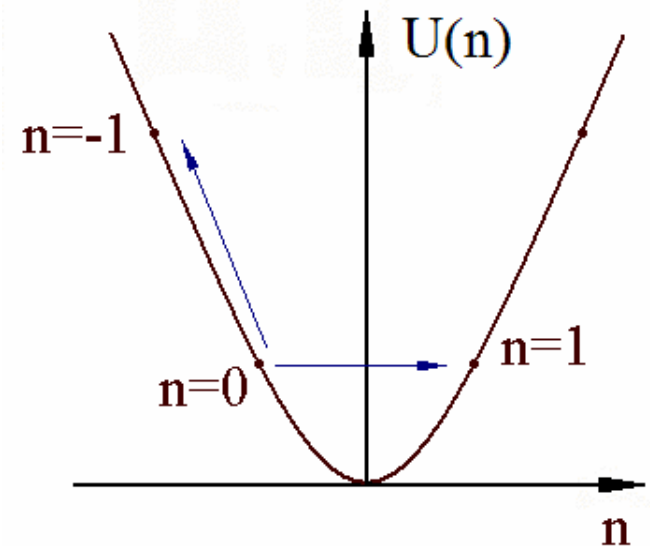
$$U(n) = E_C (n - q)^2, \quad q = CV / e.$$

$$\Delta U^\pm = U(n) - U(n \pm 1), \quad \Delta U^\pm(n=0) = \pm 2q - 1.$$

$$|q| < 1/2 \Rightarrow \Delta U^\pm < 0 \Rightarrow \Gamma(\Delta U^\pm), I \rightarrow 0.$$

### SET oscillations

$$f = I / e.$$



D.V.A. and K.K. Likharev, J. Low Temp.Phys. **62**, 345 (1986).

# Coulomb blockade in a single junction

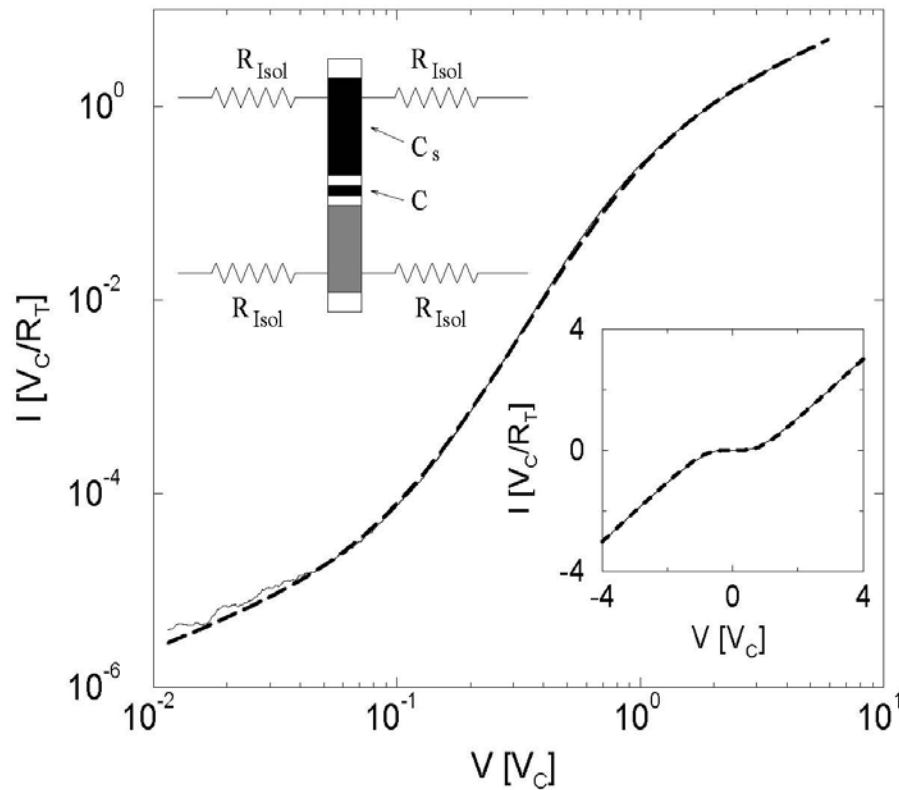


FIG. 1.  $I$ - $V$  characteristics (thin solid line) of sample 1 at 70mK compared with the theoretical fit (thick dashed line) using  $R_{Isol}$  as a free parameter. The upper inset shows the schematic of the sample, where the shaded areas are the overlapping regions formed by Al shadow evaporation and the darkest areas indicate the junctions.  $C$  and  $C_s$  are the capacitances of the main junction and the secondary junction respectively, and  $R_{Isol}$  represent the isolating resistors. The lower inset shows the linearly scaled  $I$ - $V$  curve and associated fit.

$$V \ll e/C:$$

$$I \propto V^\alpha, \quad \alpha = R/R_Q + 1.$$

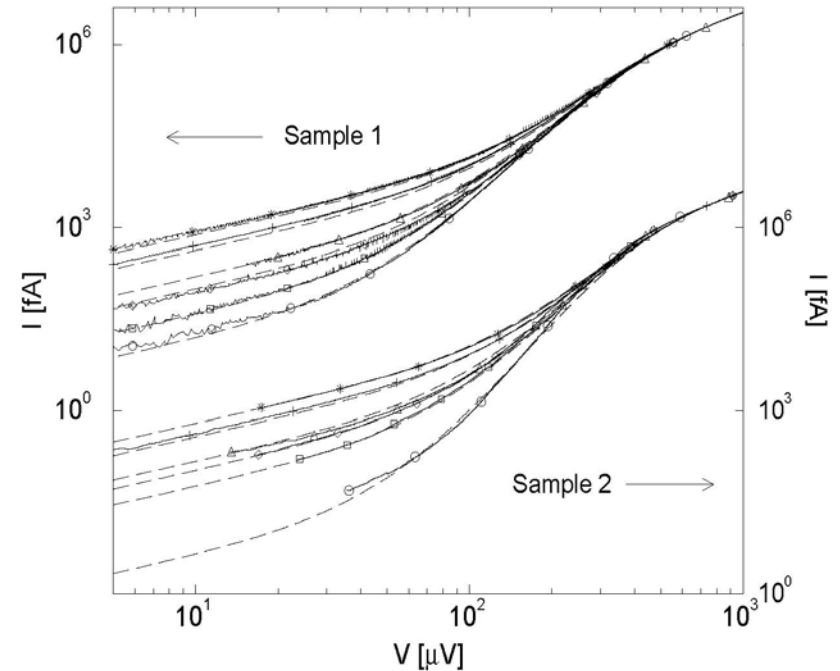
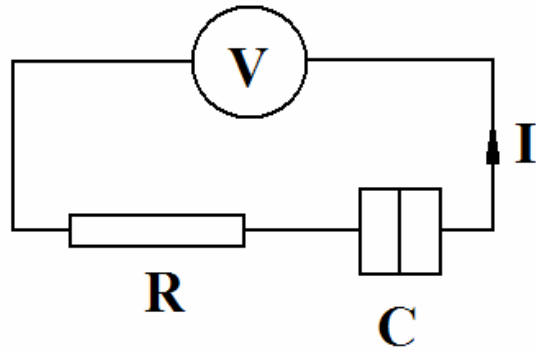


FIG. 2.  $I$ - $V$  curves at different temperatures for sample 1(2) compared with numerical results from the full theory. The temperatures are 70, 90, 118, 135, 184 and 225mK (bottom to top) for sample 1 and 75, 90, 122, 143, 195 and 225mK (bottom to top) for sample 2.

W. Zheng *et al.*, Sol. St. Comm. **108**, 839 (1998).

## Single junction



### Coulomb blockade

$$U(n) = E_C (n - q)^2, \quad q = CV / e.$$

$$\Delta U^\pm = U(n) - U(n \pm 1), \quad \Delta U^\pm(n=0) / E_C = \pm 2q - 1.$$

$$|q| < 1/2 \Rightarrow \Delta U^\pm < 0 \Rightarrow \Gamma(\Delta U^\pm), I \rightarrow 0.$$

charge decay rate  
 $1/RC$  leads to quantum  
uncertainty

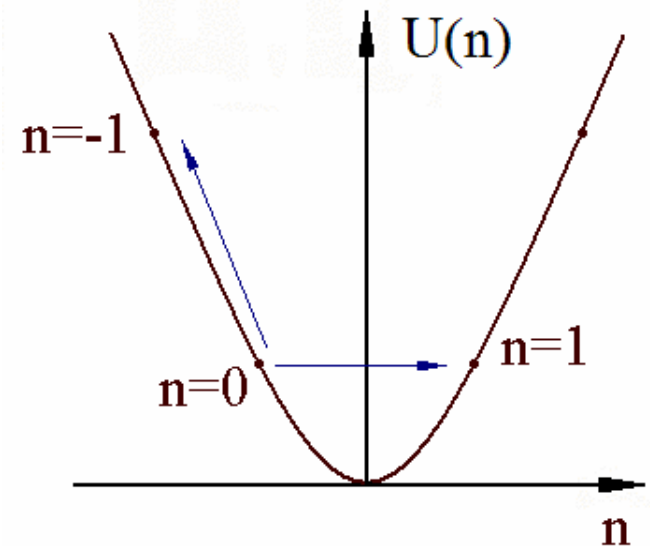
$$\hbar / RC \ll e^2 / 2C \Rightarrow$$

$$R \gg R_Q, \quad R_Q \equiv \pi \hbar / e^2 \\ \approx 13k\Omega.$$

**Duality:**  $R \leftrightarrow G$ .

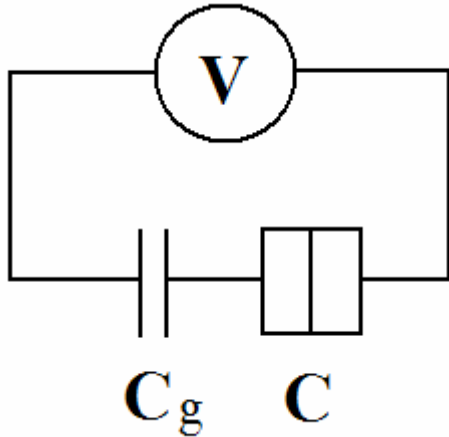
### SET oscillations

$$f = I / e.$$



D.V.A. and K.K. Likharev,  
J. Low Temp. Phys. **62**, 345 (1986).

## Single-electron box



$$U(n) = E_C (n - q)^2,$$

$$q = C_g V / e, \quad E_C = \frac{e^2}{2(C + C_g)}.$$

$$Z = \sum_n \exp\{-U(n)/T\},$$

$$\langle n \rangle = \frac{T}{2E_C} \left[ \frac{\partial}{\partial q} \ln Z + q \right].$$

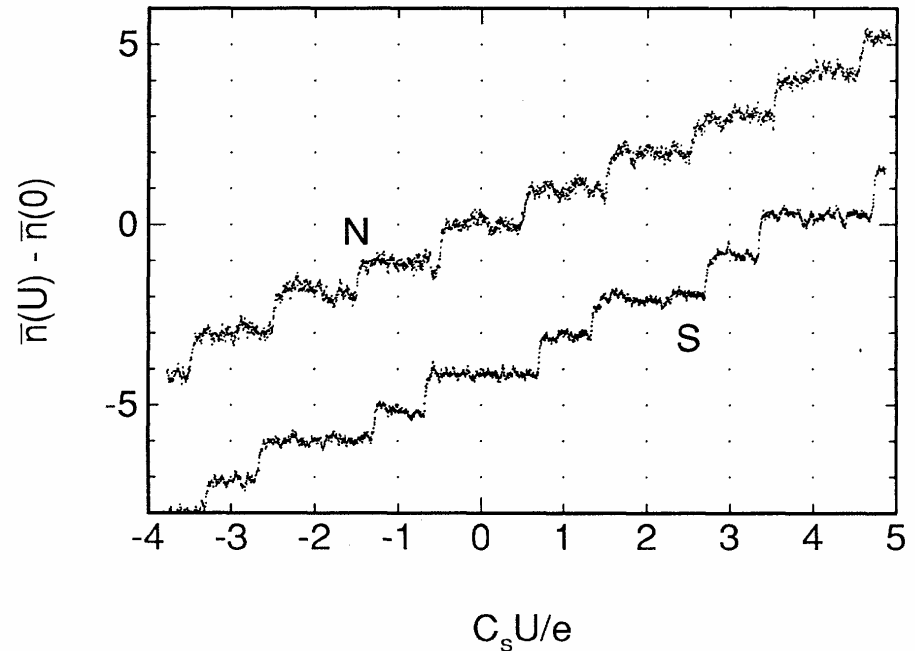
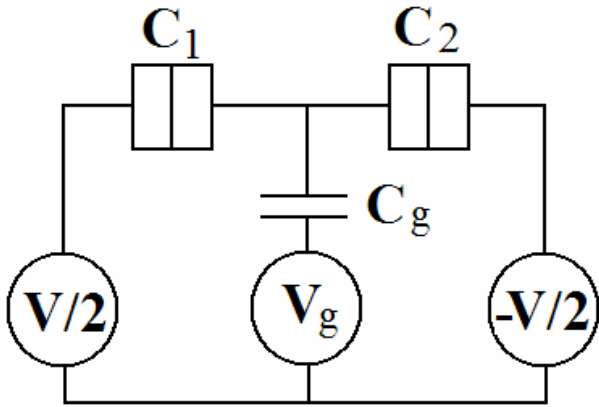


FIG. 4. Variations of the average value  $\bar{n}$  of the number of extra electrons in the box as a function of the polarization  $C_s U/e$ , at  $T = 25$  mK. Trace *N*: normal island. Trace *S*: superconducting island. For clarity, trace *S* has been offset vertically by 4 units.

P.Lafarge *et al.*, Phys. Rev. Lett. **70**, 994 (1993).

## SET transistor



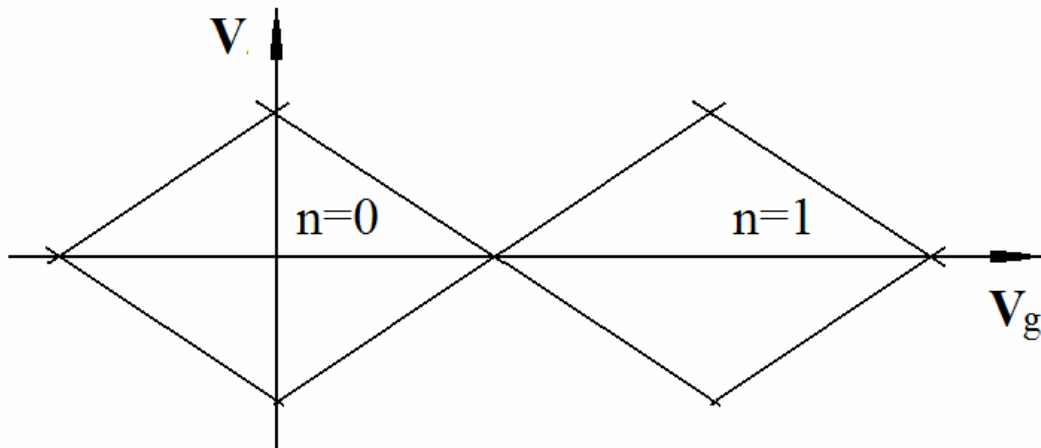
$$U(n) = E_C (n_1 - n_2 - q)^2 - (eV/2)(n_1 + n_2),$$

$$q = C_g V_g / e, \quad E_C = e^2 / 2C_\Sigma, \quad C_\Sigma = C_1 + C_2 + C_g.$$

$$\Delta U_j^\pm = U(n_j) - U(n_j \pm 1),$$

$$n = 0: \Delta U_1^\pm = \pm(eV_g C_g / C_\Sigma + eV/2) - E_C,$$

$$\Delta U_2^\pm = \mp(eV_g C_g / C_\Sigma - eV/2) - E_C.$$



D.V.A. and K.K. Likharev, J. Low Temp. Phys. **62**, 345 (1986).

T.A. Fulton and G.J. Dolan, Phys. Rev. Lett. **59**, 109 (1987).

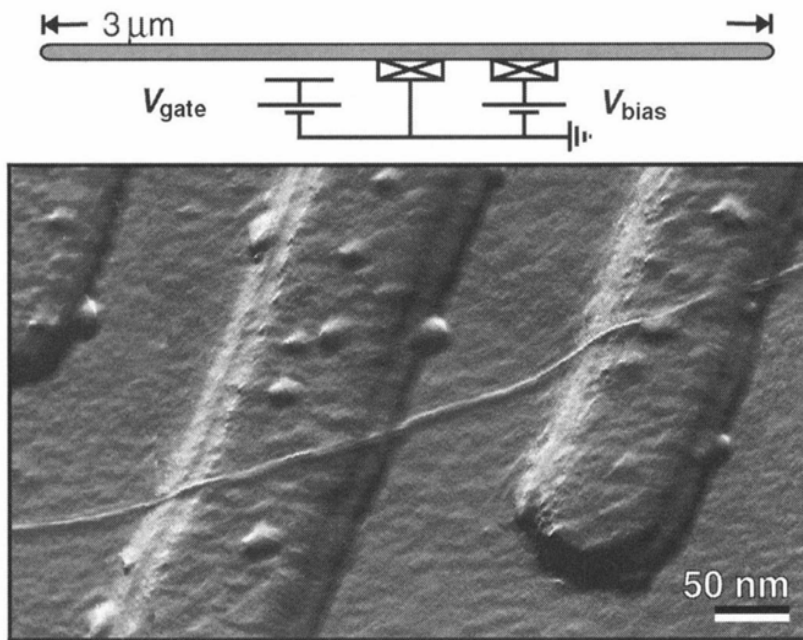


**Figure 1** AFM tapping-mode image of a carbon nanotube on top of a Si/SiO<sub>2</sub> substrate with two 15-nm-thick Pt electrodes, and a corresponding circuit diagram. The nanotubes are deposited by spin-coating of a drop of nanotube suspension. This tube has a diameter of ~1 nm, as deduced from AFM height profiles, and is identified as an individual single-wall nanotube. The total length of the tube is 3 μm, with a section of 140 nm between the contacts to which a bias voltage  $V_{\text{bias}}$  is applied. A gate voltage  $V_{\text{gate}}$  applied to the third electrode in the upper-left corner of the image is used to vary the electrostatic potential of the tube.

*S. Tans et al., Nature 386, 474 (1997).*

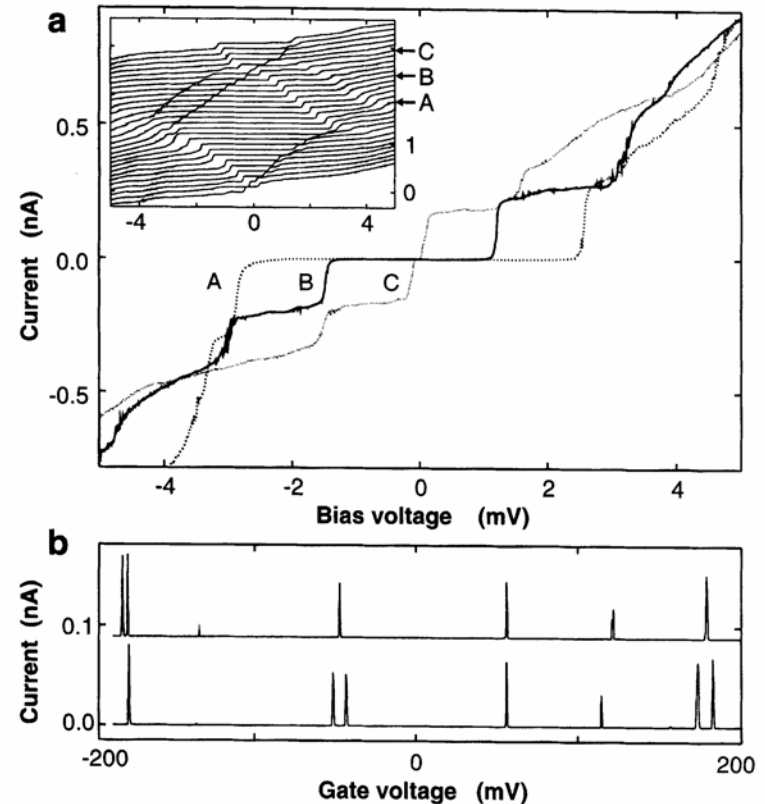


**Figure 2 a**, Current-voltage curves of the nanotube at a gate voltage of 88.2 mV (trace A), 104.1 mV (trace B) and 120.0 mV (trace C). Inset, more  $I$ - $V_{\text{bias}}$  curves with  $V_{\text{gate}}$  ranging from 50 mV (bottom curve) to 136 mV (top curve), with vertical offsets for clarity. The variation with  $V_{\text{gate}}$  of the gap around zero bias voltage implies Coulomb charging of the tube. The stepwise increase of the current at higher voltages may result from an increasing number of excited states entering in the bias window. **b**, Current versus gate voltage at  $V_{\text{bias}} = 30 \mu\text{V}$ . Two traces are shown that were performed under the same conditions.

# Periodic conductance oscillations

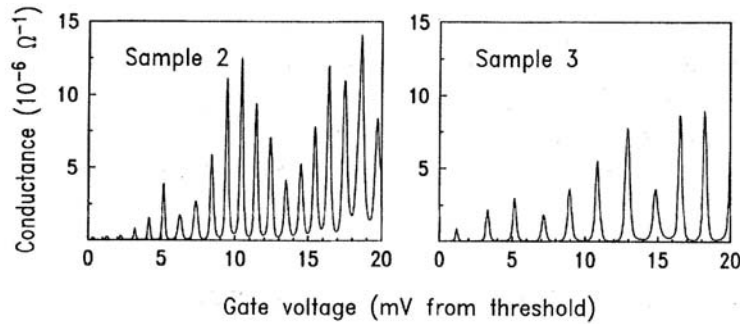
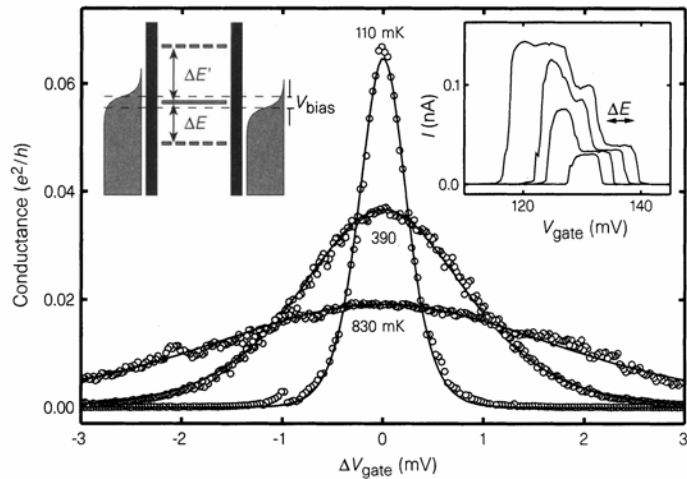


FIG. 9. Conductance as a function of  $V_g$  for two devices with different lengths: Sample 2 has  $L_0 = 0.8 \mu\text{m}$ , and sample 3 has  $L_0 = 0.6 \mu\text{m}$ . Note that samples 1(a) and 1(b) in Fig. 8 have  $L_0 = 1.0 \mu\text{m}$ . The period increases inversely with  $L_0$ .

M.A. Kastner, Rev. Mod. Phys. **64**, 849 (1992).



S. Tans *et al.*, Nature **386**, 474 (1997).

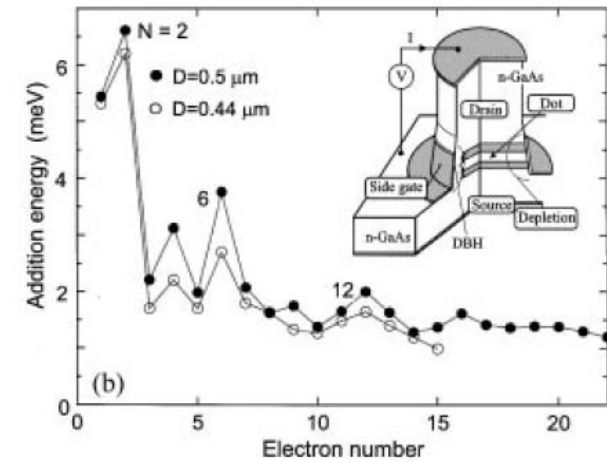
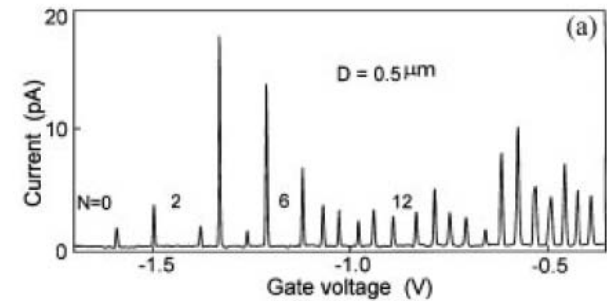
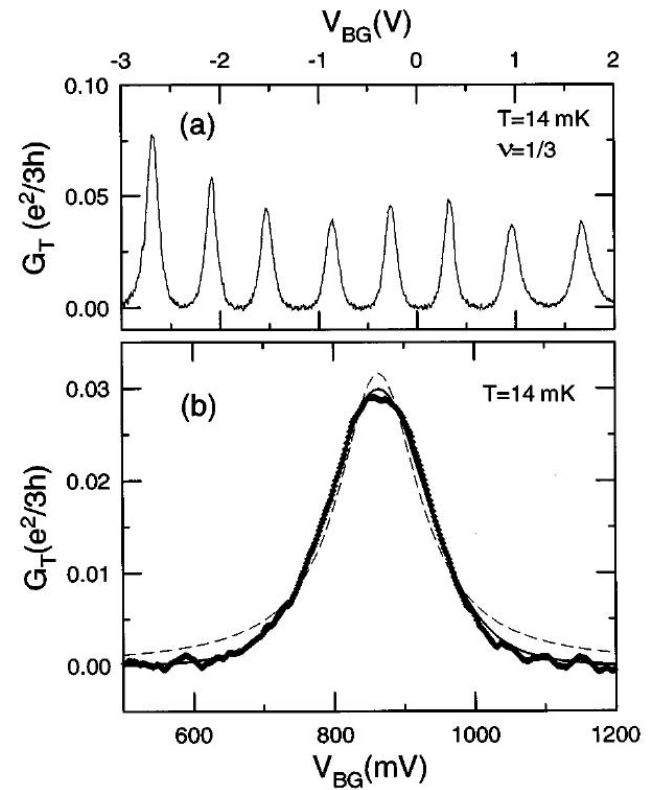
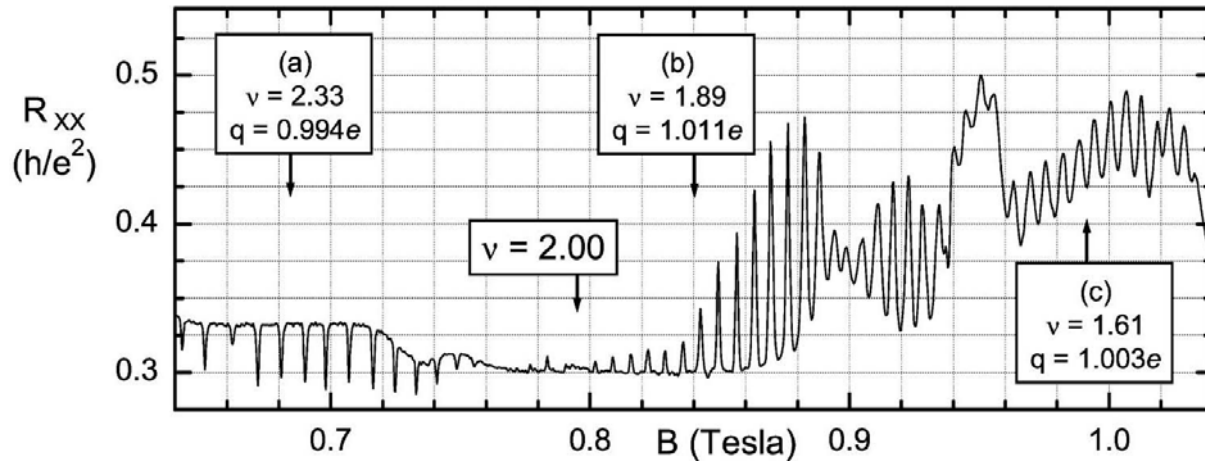
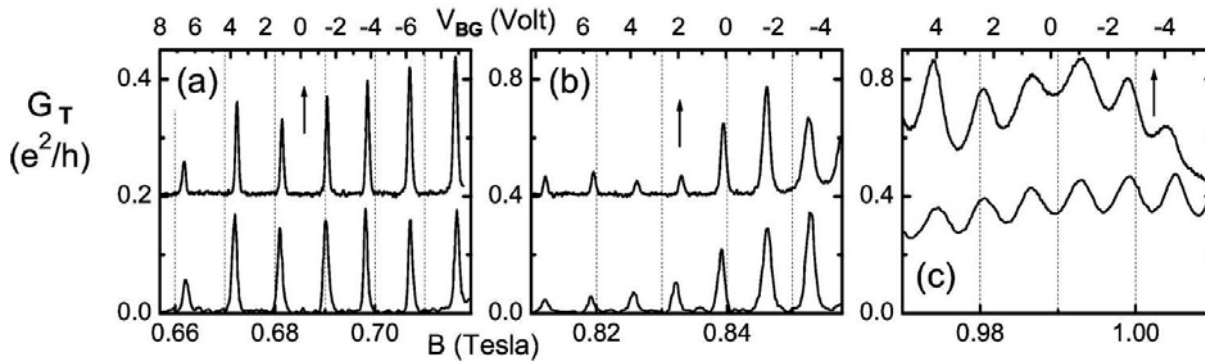
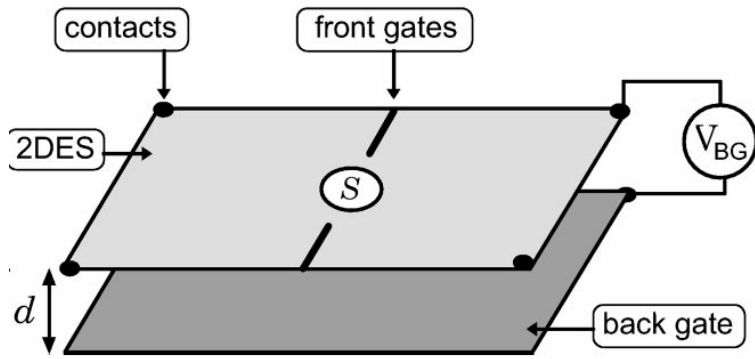


FIG. 1. (a) Coulomb oscillations in the current vs gate voltage at  $B = 0 \text{ T}$  observed for a  $D = 0.5 \mu\text{m}$  dot. (b) Addition energy vs electron number for two different dots with  $D = 0.5$  and  $0.44 \mu\text{m}$ . The inset shows a schematic diagram of the device. The dot is located between the two heterostructure barriers.

S. Tarucha *et al.*, Phys. Rev. Lett. **77**, 3613 (1996).

# Periodic conductance oscillations (2)



V.J. Goldman *et al.*,  
 Phys. Rev. B **64**,  
 085319 (2001).

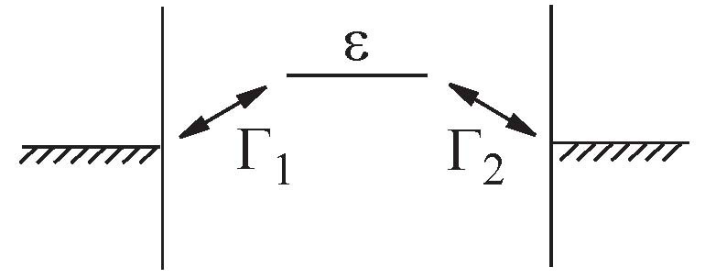
## Periodic conductance oscillations (3)

Calculation of the line-shape of the peaks

(a) balance equation:

$$\dot{p} = \Gamma^{(in)} (1 - p) - \Gamma^{(out)} p, \quad \Gamma^{(in,out)} = \sum_{j=1,2} \Gamma_j^{(in,out)}.$$

$$\dot{p} = 0: \quad p = \Gamma^{(in)} / \Gamma_{\Sigma}, \quad \Gamma_{\Sigma} = \Gamma^{(in)} + \Gamma^{(out)}.$$



(b) dc current through the level:

$$\begin{aligned} \langle I \rangle &= \Gamma_1^{(in)} (1 - p) - \Gamma_1^{(out)} p = [\Gamma_1^{(in)} \Gamma^{(out)} - \Gamma_1^{(out)} \Gamma^{(in)}] / \Gamma_{\Sigma} = \\ &= [\Gamma_1^{(in)} \Gamma_2^{(out)} - \Gamma_2^{(in)} \Gamma_1^{(out)}] / \Gamma_{\Sigma} = (1 - e^{-eV/T}) \Gamma_1^{(in)} \Gamma_2^{(out)} / \Gamma_{\Sigma}. \end{aligned}$$

(c) conductance:

$$G = e \langle I \rangle / V \big|_{V \rightarrow 0} = \frac{e^2}{T} \left[ \Gamma_1^{(in)} \Gamma_2^{(out)} / \Gamma_{\Sigma} \right]_{V=0}.$$

## Periodic conductance oscillations (4)

Results:

$\hbar\Gamma \ll T \ll \delta$ :

$$\Gamma_{\Sigma} = \Gamma_1 + \Gamma_2, \quad \Gamma_1^{(in)}\Gamma_2^{(out)} = \Gamma_1\Gamma_2 f(\varepsilon)(1 - f(\varepsilon)) = \Gamma_1\Gamma_2 / 4 \cosh^2(\varepsilon / 2T),$$

$$G = \frac{\Gamma_1\Gamma_2}{\Gamma_1 + \Gamma_2} \frac{e^2}{4T \cosh^2(\varepsilon / 2T)}.$$

$\delta \ll T \ll E_C$ :

$$\Gamma_{\Sigma} = (\varepsilon / e^2)(G_1 + G_2) \coth(\varepsilon / 2T),$$

$$\Gamma_1^{(in)}\Gamma_2^{(out)} = (\varepsilon / e^2)^2 G_1 G_2 / [4 \sinh^2(\varepsilon / 2T)]$$

$$G = \frac{G_1 G_2}{2(G_1 + G_2)} \frac{\varepsilon / T}{\sinh(\varepsilon / T)}.$$

# Cotunneling

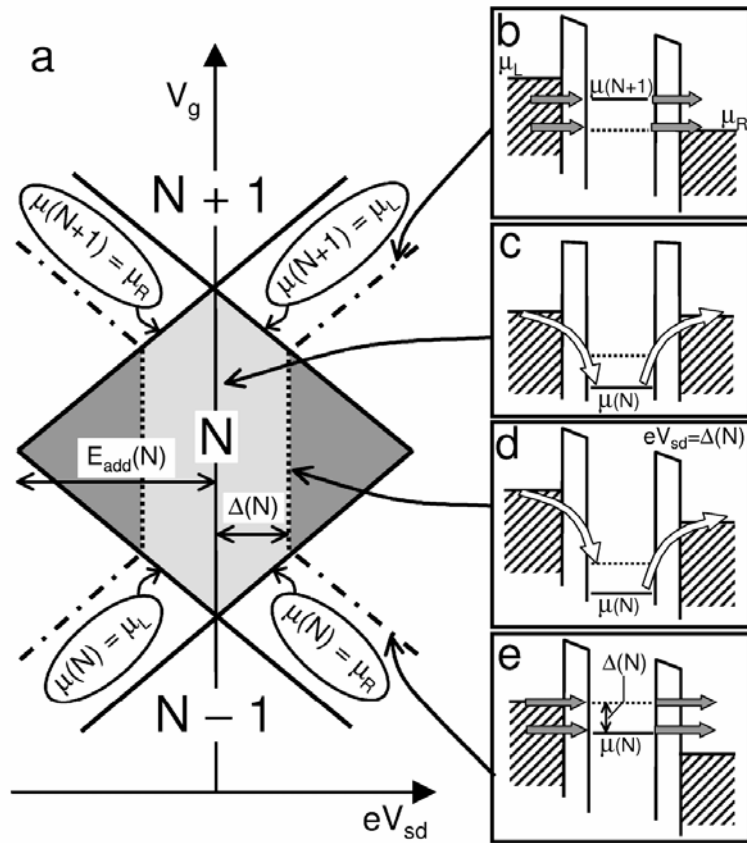


FIG. 1. (a) Stability diagram in the plane of  $(V_{sd}, V_g)$ . Angled lines correspond to *alignment* of a dot level with the Fermi energy of the leads. In this case, first-order tunneling sets in, or is increased, as illustrated in (b) and (e). In the light grey area in (a), conduction is due to elastic cotunneling via virtual events as shown in (c). For  $eV_{sd} \geq \Delta(N)$ , inelastic processes, illustrated in (d), increase the cotunneling current (dark grey areas).  $\Delta(N)$  is the energy spacing between the ground state and the first excited state, which in (b)–(e) are represented by solid and dotted lines, respectively.

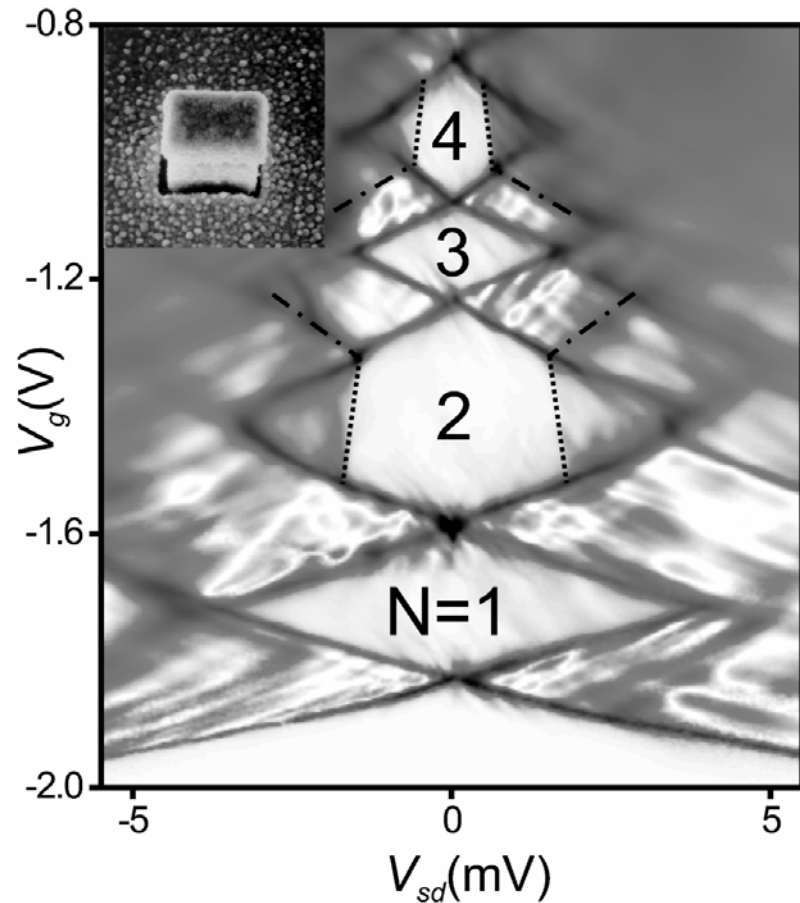
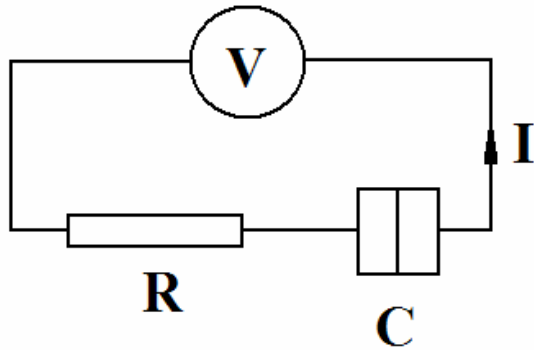


FIG. 2. Measured stability diagram of our quantum dot at 15 mK and zero magnetic field.  $dI/dV_{sd}$  is plotted in grey scale as a function of  $(V_{sd}, V_g)$ . Dotted lines have been superimposed to highlight the onset of inelastic cotunneling. The dot-dashed lines indicate the onset of first-order tunneling via an excited state. Inset: scanning electron micrograph of the device.

S. De Franceschi *et al.*, Phys. Rev. Lett. **86**, 878 (2001).

## Single junction



### Coulomb blockade

$$U(n) = E_C (n - q)^2, \quad q = CV / e.$$

$$\Delta U^\pm = U(n) - U(n \pm 1), \quad \Delta U^\pm(n=0) / E_C = \pm 2q - 1.$$

$$|q| < 1/2 \Rightarrow \Delta U^\pm < 0 \Rightarrow \Gamma(\Delta U^\pm), I \rightarrow 0.$$

charge decay rate  
 $1/RC$  leads to quantum  
 uncertainty

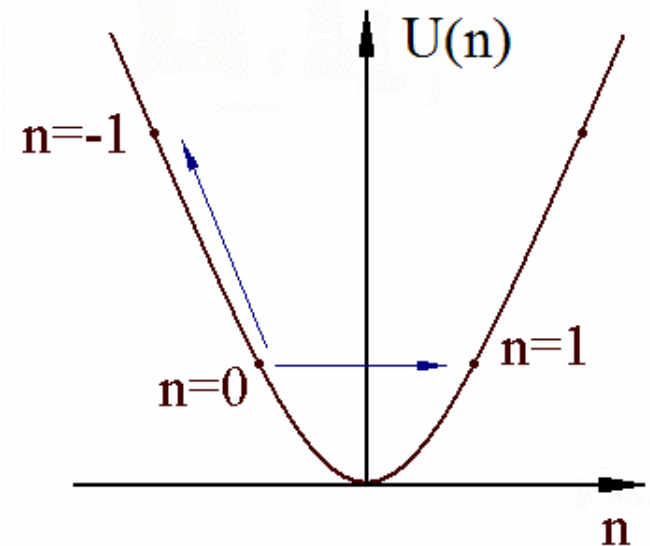
$$\hbar / RC \ll e^2 / 2C \Rightarrow$$

$$R \gg R_Q, \quad R_Q \equiv \pi \hbar / e^2 \\ \approx 13k\Omega.$$

**Duality:**  $R \leftrightarrow G.$

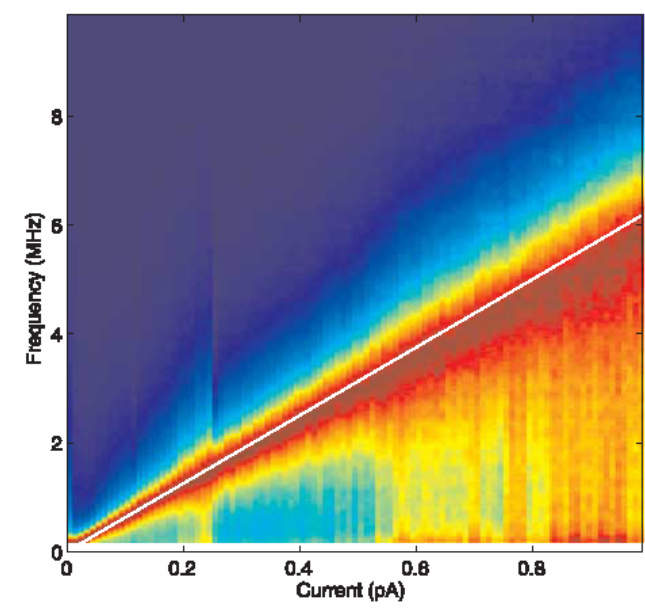
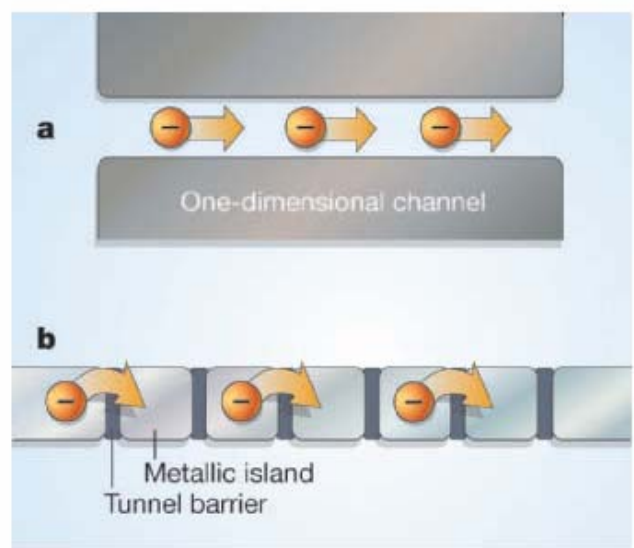
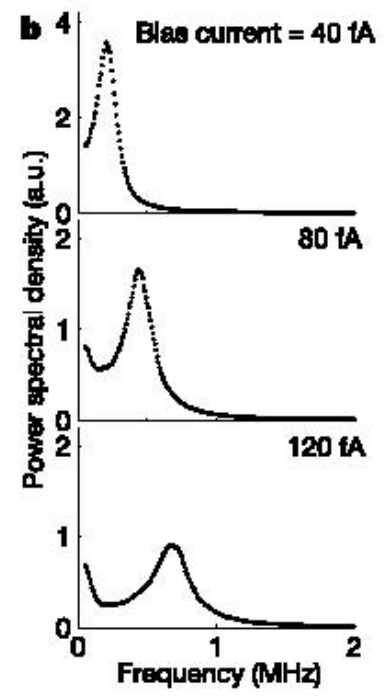
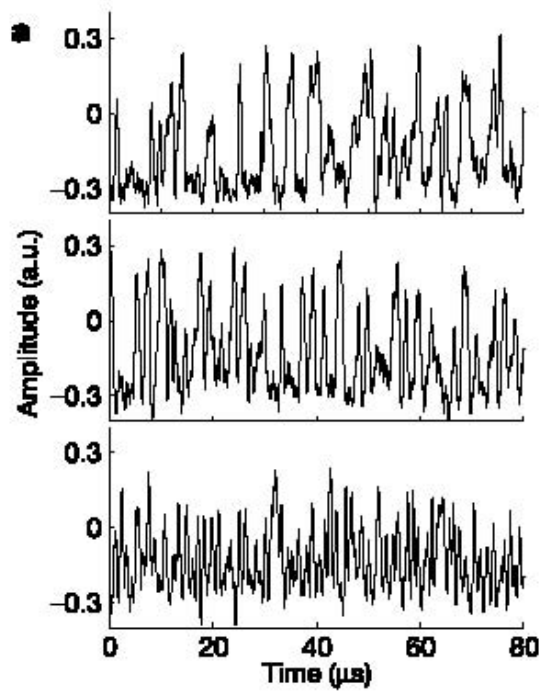
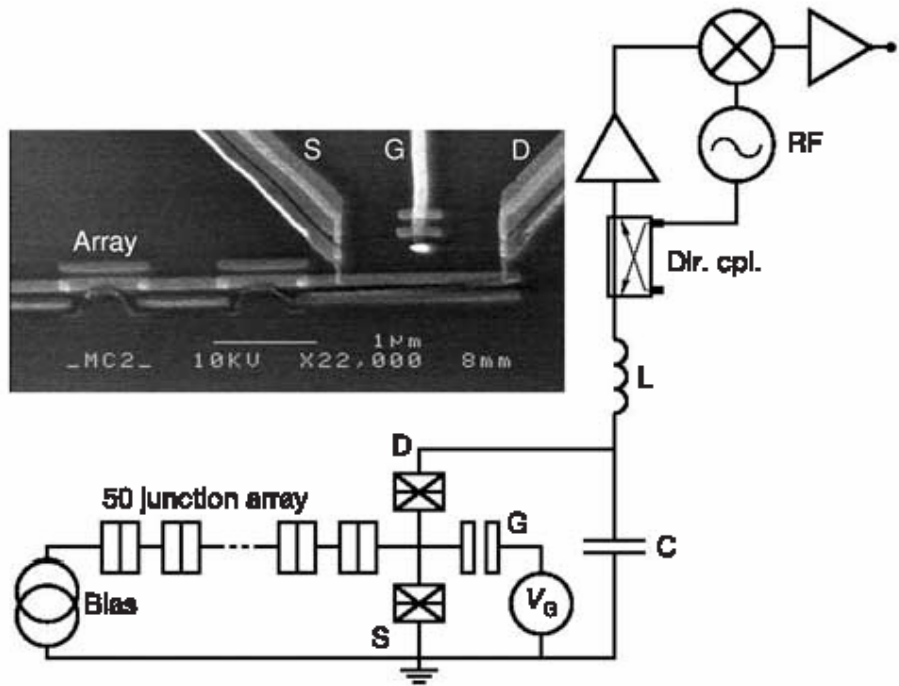
### SET oscillations

$$f = I / e.$$



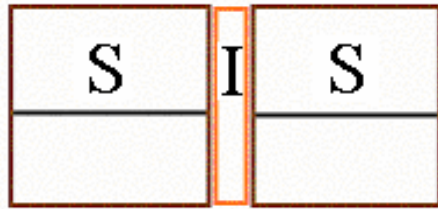
D.V.A. and K.K. Likharev,  
 J. Low Temp. Phys. **62**, 345 (1986).

# SET oscillations



J. Bylander *et al.*, Nature **434**, 361 (2005).

## Cooper-pair tunneling



For tunnel junction; energies smaller than the superconducting gap  $\Delta$ , Cooper-pair tunneling is distinguished from the quasiparticle tunneling

Classical Josephson dynamics:

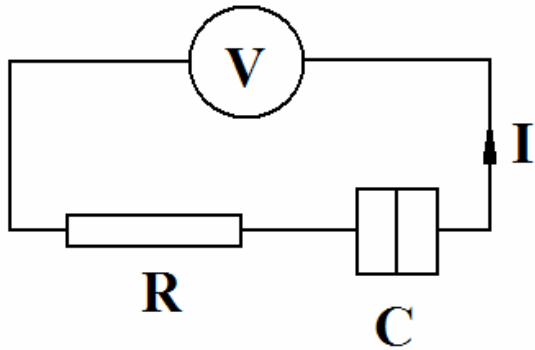
$$I = I_C \sin \varphi; \quad \dot{\varphi} = (2e/\hbar)V \quad \Leftrightarrow \quad H = Q^2 / 2C - E_J \cos \varphi, \quad \{\Phi, Q\} = 1,$$
$$\Phi = (\hbar/2e)\varphi, \quad E_J = (\hbar/2e)I_C, \quad Q = CV.$$

Quantization:

$$[\Phi, Q] = i\hbar \quad \Rightarrow \quad [\varphi, Q] = 2ei,$$
$$H = Q^2 / 2C - E_J/2 (|Q\rangle\langle Q \pm 2e| + |Q \pm 2e\rangle\langle Q|).$$

$\psi(\varphi + 2\pi) =, \neq \psi(\varphi) \quad \Leftrightarrow \quad \text{continuous versus discrete charge } Q$

## Single junction

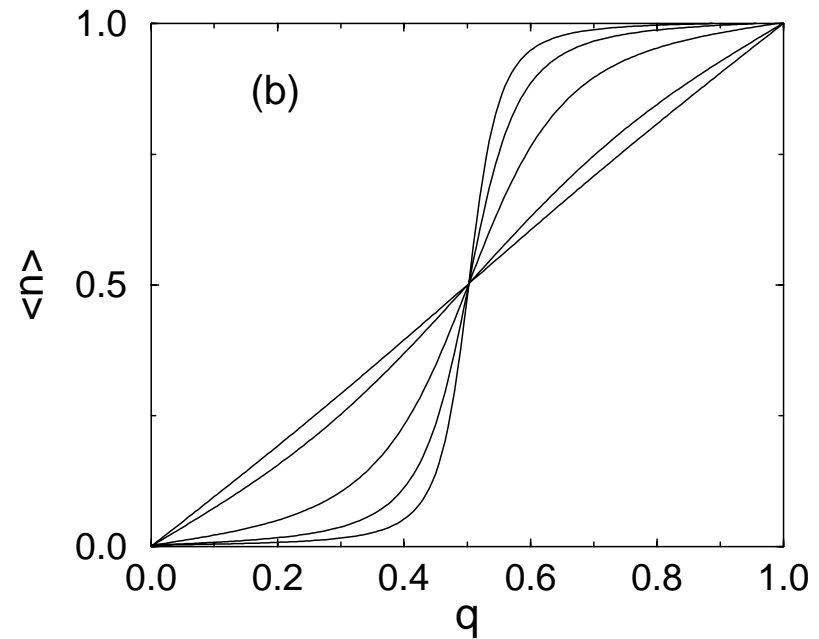
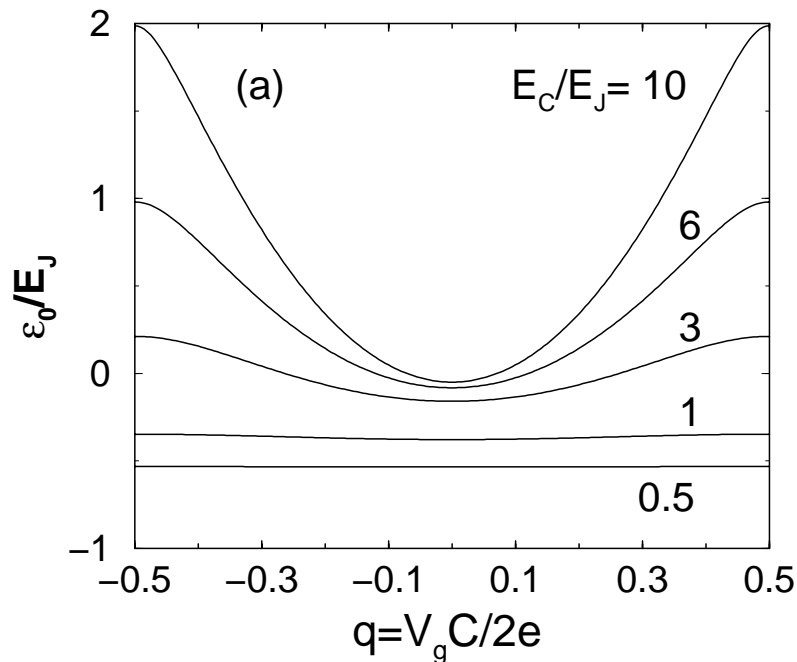


$$Q = 2e(n - q), \quad q = \int I dt.$$

$$H = E_C(n - q)^2 - E_J/2(|n\rangle\langle n \pm 1| + |n \pm 1\rangle\langle n|),$$

$$E_C = (2e)^2 / 2C.$$

## Bloch oscillations $f = I / 2e$ .



D.V.A., A.B. Zorin, and K.K. Likharev,  
Sov. Phys. JETP **61**, 407 (1985).

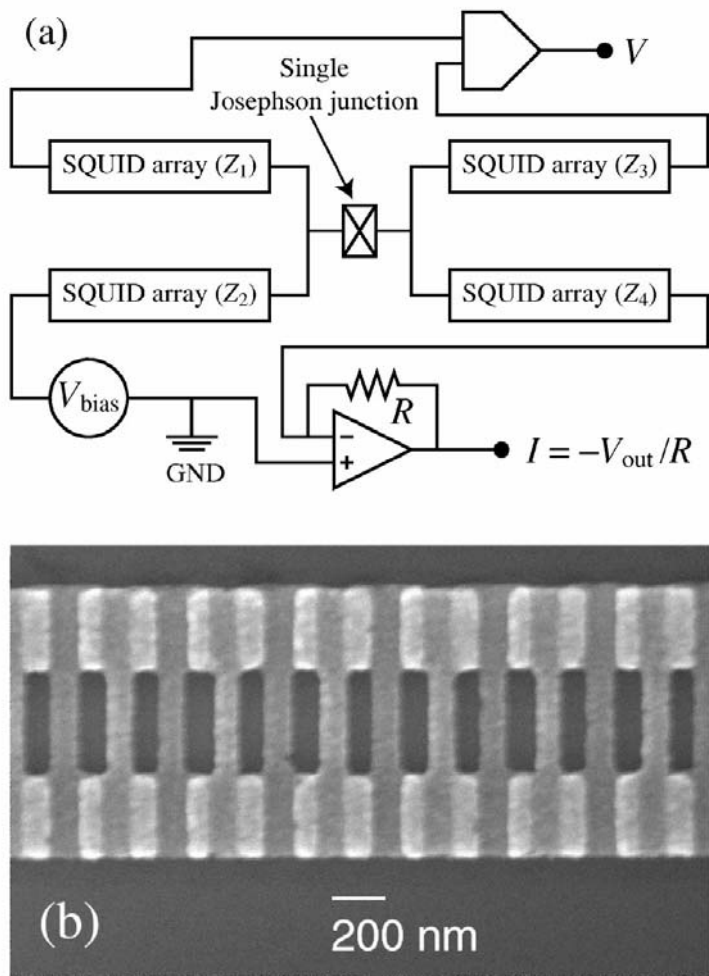


FIG. 2. (a) Schematic diagram of the samples and the circuit for measurements. (b) Scanning electron micrograph of a part of the 1D SQUID array.

M. Watanabe and D.B. Haviland,  
PRB 67, 094505 (2003).

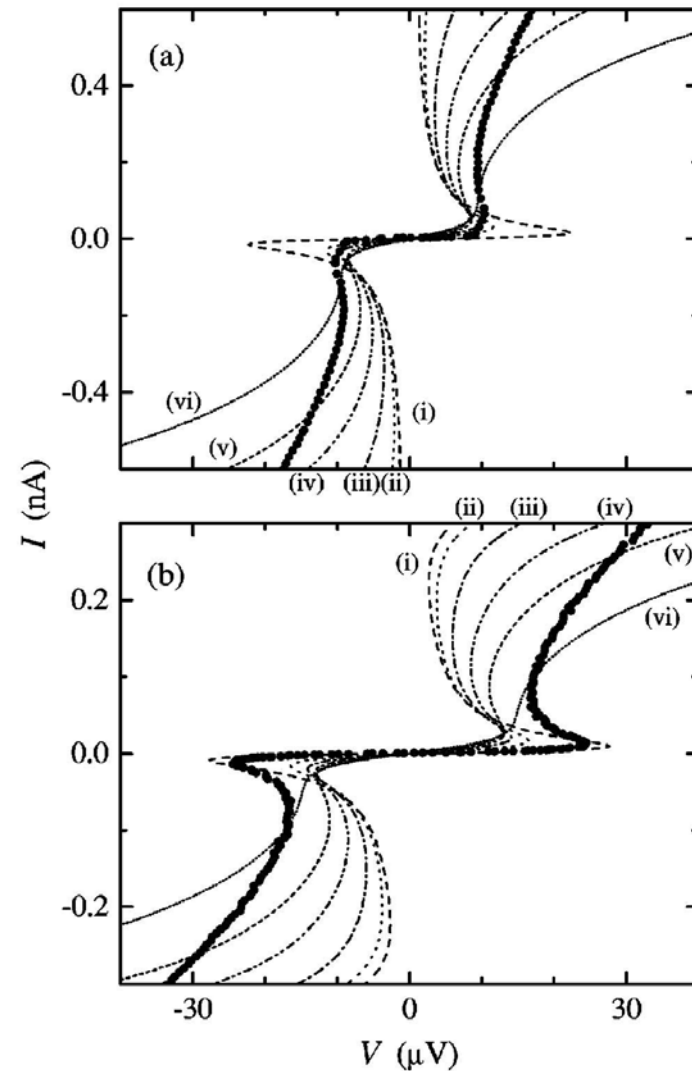
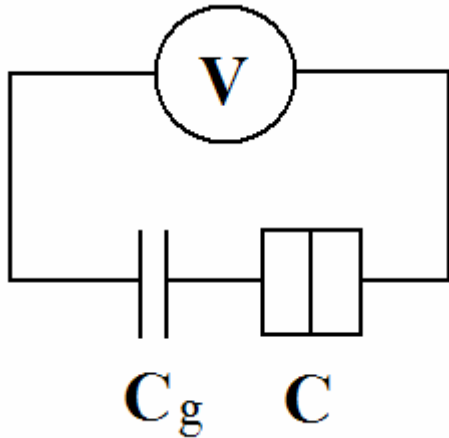


FIG. 9. Current-voltage curves of single Josephson junctions. (a) The measured curve (solid circles) of sample G at  $T=0.04$  K and  $f=0.46$  is compared with the numerical calculations for  $E_J/E_C=0.53$  and  $\alpha=0.006$  [see Eqs. (10) and (16) for the definition of  $\alpha$  and  $f$ , respectively]. (b) sample I at  $T=0.02$  K and  $f=0.49$  with the calculations for  $E_J/E_C=0.99$  and  $\alpha=0.003$ . For both the figures,  $C=1.3$  fF is assumed in the calculations, and from (i) to (vi),  $k_B T/E_C=0.05, 0.3, 0.4, 0.5, 0.6$ , and  $0.8$ , respectively.

## Cooper-pair box



$$H = E_C (n - q)^2 - E_J \cos \varphi,$$

$$q = C_g V / 2e, \quad E_C = \frac{2e^2}{C + C_g}.$$

$$Z = \text{Tr} \left[ e^{-H/T} \right]$$

$$\langle n \rangle = \frac{T}{2E_C} \left[ \frac{\partial}{\partial q} \ln Z + q \right].$$

M. Buttiker, PRB **36**, 3548 (1987).

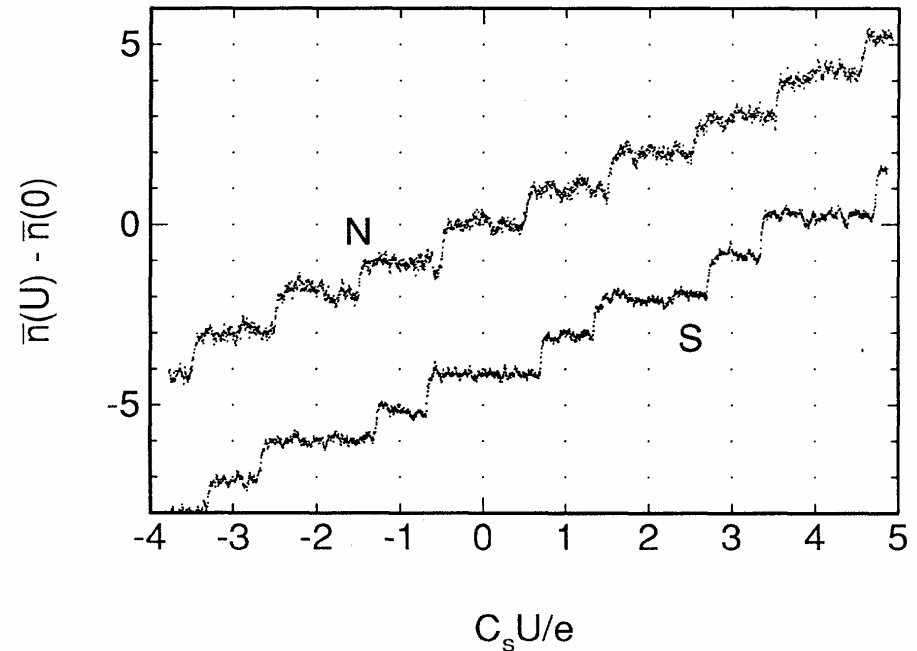
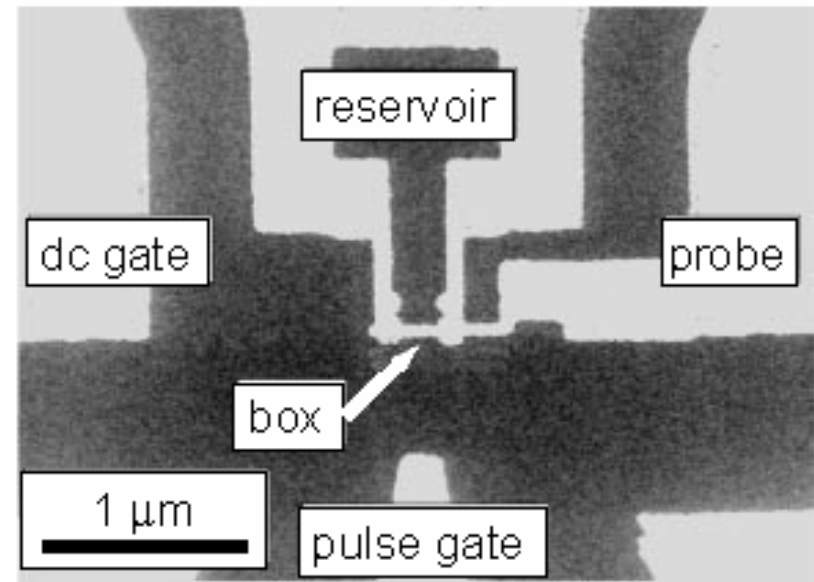
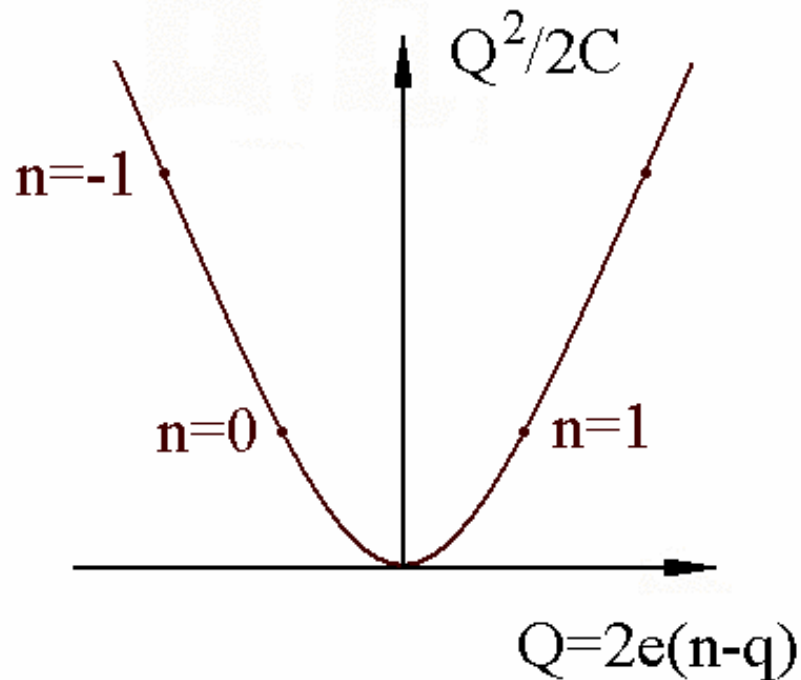


FIG. 4. Variations of the average value  $\bar{n}$  of the number of extra electrons in the box as a function of the polarization  $C_s U/e$ , at  $T = 25$  mK. Trace *N*: normal island. Trace *S*: superconducting island. For clarity, trace *S* has been offset vertically by 4 units.

P. Lafarge *et al.*, PRL **70**, 994 (1993).

## Cooper-pair box as charge qubit

$$E_J \ll E_C, \quad q \approx 1/2$$



$$H = -E_C(q - 1/2)\sigma_z - (E_J/2)\sigma_x$$

Y. Nakamura *et al.*,  
Nature **398**, 786 (1999).